X-ray linear dichroism in an α,ω-dibromoalkane/urea inclusion compound and its application to polarization analysis of magnetic diffraction

2002 J. Phys.: Condens. Matter 14 123

(http://iopscience.iop.org/0953-8984/14/1/311)

INSTITUTE OF PHYSICS PUBLISHING JOURNAL OF PHYSICS: CONDENSED MATTER

J. Phys.: Condens. Matter **14** (2002) 123–134 PII: S0953-8984(02)29290-5

X-ray linear dichroism in an α, ω-dibromoalkane/urea inclusion compound and its application to polarization analysis of magnetic diffraction

S P Collins[1], D Laundy[1], K D M Harris[2], B M Kariuki[2], C L Bauer[2], S D Brown[3] and P Thompson[3]

[1] Daresbury Laboratory, Warrington WA4 4AD, UK
[2] School of Chemistry, University of Birmingham, Edgbaston, Birmingham B15 2TT, UK
[3] XMaS UK CRG, ESRF, BP 220, F-38043 Grenoble Cédex, France

E-mail: s.p.collins@daresbury.ac.uk and k.d.m.harris@bham.ac.uk

Received 26 September 2001
Published 7 December 2001
Online at stacks.iop.org/JPhysCM/14/123

Abstract

We report the first polarization analysis of magnetic x-ray diffraction using a dichroic polarization analyser. The α, ω-dibromoalkane/urea inclusion compounds are shown to produce highly effective dichroic filters for fixed-wavelength (bromine K-edge) applications. We discuss the dichroic properties of these materials and show that devices which exploit linear dichroism can offer some important advantages over diffraction-based polarization analysers.

1. Background

One of the earliest, and most compelling, promises of the emerging technique of magnetic x-ray diffraction was the ability to provide *separate* spin and orbital densities in magnetic crystals. Such data are of crucial importance for modelling magnetism in bulk materials and thin films, and, for example, understanding the microscopic origins of magnetic anisotropy. Despite the initial interest, and the fact that non-resonant magnetic diffraction is the only known technique for extracting spin and orbital densities, progress in this area has been disappointing.

Measurements on ferromagnetic crystals [1] are difficult, due to the requirement for field and/or circular polarization 'flipping', neither of which is without technical complication. For studies of pure antiferromagnetic diffraction, one can extract information about spin/orbital ratios by linear polarization analysis of the scattered beam, as first demonstrated by Gibbs *et al* [2]. While a few successful measurements based on this technique have been reported [3, 4], data quality has rarely exceeded that of the early experiments. Measurements of this kind are extremely challenging, due to the very weak diffraction signals (often well below 10^{-6} of the structural scattering), combined with the low average transmittance of diffraction-based linear polarization analysers. Moreover, while the polarization extinction

ratios are typically very high for $2\theta \sim 90^\circ$ scattering by the analyser crystal, the devices can be complicated to use, often require wasteful 'rocking' of the analyser crystal, and can be prone to systematic errors arising from misalignment and variations in beam divergence and crystal quality.

Although the intensities from non-resonant magnetic diffraction are typically very low, the polarization variations of interest can be significant. Under such circumstances, a useful polarization analyser is one which has a high average transmittance while being relatively insensitive to beam divergence and angular variations, but where the requirement for high polarization extinction ratios can be relaxed. These features are precisely the characteristics of a polarization filter based on x-ray linear dichroism. The present work focuses on the use of bromine K-edge linear dichroism in α, ω-dibromoalkane/urea inclusion compounds for linear polarization analysis. The properties of such materials, and their fabrication into x-ray polarization filters, is discussed, and we report the results of the first dichroic polarization analysis of magnetic diffraction, in the form of a short study of antiferromagnetic holmium.

2. Principles and theory

2.1. Magnetic scattering

The scattering amplitudes, polarization dependence and cross-sections for non-resonant magnetic x-ray diffraction are discussed in some detail in the literature [2, 5, 6], so we will reproduce only key results of relevance to the present work. The average polarization of the diffracted beam, defined by a set of Stokes parameters, depends on Fourier components of the spin and orbital magnetization densities, as well as wavelength and sample orientation. Typically, the scattering plane of the experiment will be either parallel or perpendicular to the direction of net linear polarization, giving $P_1 = 0$, where P_1 is the Stokes parameter for polarization at 45° from the scattering plane. Also it is often safe to assume that there is no net circular polarization in the incident beam, i.e., $P_2 = 0$. For the diffracted beam, we are concerned with the degree of linear polarization perpendicular to the scattering plane, which we denote as P_3'. Applying standard density-matrix techniques, one can readily formulate an expression for the required Stokes parameter:

$$P_3' = \frac{(1+P_3)\,(I_{\sigma\sigma} - I_{\sigma\pi}) + (1-P_3)\,(I_{\pi\sigma} - I_{\pi\pi})}{(1+P_3)\,(I_{\sigma\sigma} + I_{\sigma\pi}) + (1-P_3)\,(I_{\pi\sigma} + I_{\pi\pi})} \tag{1}$$

where the intensities (or cross-sections) for the various polarization channels, far from any absorption edge resonance of the magnetic sample, are

$$\begin{aligned} I_{\sigma\sigma} &= |S_2 \sin 2\theta|^2 \qquad & I_{\pi\sigma} &= |2\sin^2\theta[S_3\sin\theta - (L_1+S_1)\cos\theta]|^2 \\ I_{\sigma\pi} &= |2\sin^2\theta[S_3\sin\theta + (L_1+S_1)\cos\theta]|^2 \qquad & I_{\pi\pi} &= |\sin 2\theta[2\sin^2\theta\ L_2 + S_2]|^2. \end{aligned} \tag{2}$$

For diffraction measurements, S_j, L_j are Fourier components of the spin and orbital angular momentum density along the three coordinate axes, defined in [6].

Considering the specific example of the holmium spiral antiferromagnetic phase, the magnetization direction is described by a unit vector, $\hat{\boldsymbol{m}}$, in the basal plane of the hcp structure, which rotates from one atomic layer to the next. For reflections along the $00L$ direction, the z-axis is normal to the basal plane, and we can write

$$\hat{\boldsymbol{m}}(\boldsymbol{r}) = \begin{pmatrix} \cos(\boldsymbol{\tau}\cdot\boldsymbol{r}) \\ \sin(\boldsymbol{\tau}\cdot\boldsymbol{r}) \\ 0 \end{pmatrix} \tag{3}$$

where $\boldsymbol{\tau}$ is the magnetic modulation wave-vector, which lies parallel to $\boldsymbol{c}^*$. Writing the spin and orbital Fourier components as

$$\boldsymbol{S}(\boldsymbol{k}) = \begin{pmatrix} S(k) \\ \pm \mathrm{i} S(k) \\ 0 \end{pmatrix} \qquad \boldsymbol{L}(\boldsymbol{k}) = \begin{pmatrix} g(k)S(k) \\ \pm \mathrm{i} g(k)S(k) \\ 0 \end{pmatrix} \tag{4}$$

where $g(k)$ is the ratio of the spin to orbital Fourier component along the magnetic unit vector, the relevant expression for the degree of linear polarization becomes

$$P_3' = \frac{(1+P_3)\left(1-\sin^2\theta(1+g(k))^2\right)+(1-P_3)\left(\sin^2\theta(1+g(k))^2-(1+2\sin^2\theta\ g(k))^2\right)}{(1+P_3)\left(1+\sin^2\theta(1+g(k))^2\right)+(1-P_3)\left(\sin^2\theta(1+g(k))^2+(1+2\sin^2\theta\ g(k))^2\right)}. \tag{5}$$

If P_3 and θ are known, then $g(k)$ can be extracted from a measurement of P_3'. For holmium, with a more-than-half-filled 4f shell with $L = 6$, $S = 2$ in the Hund-rule ground state, one can write [2]

$$g(k) = \frac{\boldsymbol{L}\cdot\boldsymbol{J}}{\boldsymbol{S}\cdot\boldsymbol{J}}\frac{f_l(k)}{f_s(k)} = 3\frac{f_l(k)}{f_s(k)} \tag{6}$$

where $f_l(k)$ and $f_s(k)$ are the orbital and spin magnetic form factors, respectively.

The $0\,0\,L \pm \tau$ reflections from the spiral structure of holmium are simple to interpret because they are independent of the azimuthal rotation angle about the scattering vector. However, for other reflections this is generally not the case, and one must consider the precise orientation of the magnetic structure. Changing from one reflection, which we call the *primary* reflection, to another (the *secondary* reflection) implies a change of coordinate system, which can be achieved conveniently by applying three rotations as follows: (1) rotate by an angle β about the z-axis to ensure that the primary and secondary reciprocal-lattice vectors both lie in the scattering plane, (2) rotate by an angle α about the y-axis to align the secondary reflection to the diffraction condition, (3) perform a second rotation about the z-axis, by an angle ψ, to select the required azimuthal setting of the secondary reflection. These operations combine to give the unitary transformation matrix

$$\begin{aligned} R_3(\psi)R_2(\alpha)R_3(\beta) = &\begin{pmatrix} \cos(\psi) & -\sin(\psi) & 0 \\ \sin(\psi) & \cos(\psi) & 0 \\ 0 & 0 & 1 \end{pmatrix} \\ &\times \begin{pmatrix} \cos(\alpha) & 0 & \sin(\alpha) \\ 0 & 1 & 0 \\ -\sin(\alpha) & 0 & \cos(\alpha) \end{pmatrix} \begin{pmatrix} \cos(\beta) & -\sin(\beta) & 0 \\ \sin(\beta) & \cos(\beta) & 0 \\ 0 & 0 & 1 \end{pmatrix}. \end{aligned} \tag{7}$$

Here, α is the angle between the primary and secondary reciprocal-lattice vectors. For the present case, these are $00L$ and $\bar{2}1L$, and one can write

$$\cos(\alpha) = \frac{L}{\sqrt{L^2 + 4(c/a)^2}} \tag{8}$$

where a and c are the hexagonal unit-cell parameters. Computing the linear polarization for an arbitrary orientation is then simply a matter of applying equations (1)–(4) with

$$\boldsymbol{S}(\boldsymbol{k}) \rightarrow R_3(-\beta)R_2(-\alpha)R_3(-\psi)\boldsymbol{S}(\boldsymbol{k}) \tag{9}$$

and similarly for $\boldsymbol{L}(\boldsymbol{k})$.

Measurement of the linear polarization is achieved with a dichroic polarizer, placed between the sample and the x-ray detector. Assuming again $P_1' = P_2' = 0$, the intensity transmitted by a polarizer of *principal transmittance ratio* [7] R_t (the ratio of maximum to

minimum intensity transmitted through the device with linearly polarized incident beam), aligned with the major axis at an angle $\boldsymbol{\eta}$ from the scattering plane, is

$$I \propto (R_t + 1) + P_3'(R_t - 1)\cos 2\boldsymbol{\eta} \propto \left(1 + \Phi\, P_3' \cos 2\boldsymbol{\eta}\right) \tag{10}$$

from which one can write

$$P_3' = \frac{1}{\Phi}\frac{R_I - 1}{R_I + 1} \tag{11}$$

where

$$\Phi = \frac{R_t - 1}{R_t + 1}$$

and R_I is the ratio of intensities measured with $\boldsymbol{\eta} = 0^\circ$ and 90°. P_3' can therefore be extracted from polarizer intensity ratios given the value of Φ. This in turn can be extracted from equation (10) via a measurement with *known* polarization, made, for example, using the incident x-ray beam, or (as in the present case) non-magnetic scattering, for which the scattered beam linear polarization is

$$P_3' = \frac{P_3 + \frac{1}{2}\sin^2 2\theta(1 - P_3)}{1 - \frac{1}{2}\sin^2 2\theta(1 - P_3)}. \tag{12}$$

A precise measurement of P_3' requires a polarizer with both a high average transmittance and a high principal transmittance ratio.

2.2. Linear dichroism in α, ω-dibromoalkane/urea inclusion compounds

Strong linear dichroism has been observed at the bromine K edge in a number of systems in which there are highly oriented bonds involving bromine. Sharp 'white-line' features are found at the absorption edge, corresponding to the filling of the only available 4p state—the empty anti-bonding σ^*-orbital. A net orientation of such bonds can be found in stretched polymers [8] or highly anisotropic crystal environments [9].

The present work exploits the dichroic properties of α, ω-dibromoalkane/urea inclusion compounds, in which the α, ω-dibromoalkane guest molecules ($Br(CH_2)_nBr$) occupy the parallel c-axis tunnels of the hexagonal urea host structure [10–12]. In this paper, we focus on the case with $n = 10$—i.e. 1,10-dibromodecane ($Br(CH_2)_{10}Br$). The α, ω-dibromoalkane guest molecules (figure 1) are thus highly oriented parallel to the crystal c-axis. However, at room temperature they are disordered with respect to rotation about this axis [13,14]. The C–Br bond lies at an angle ξ from the c-axis which is close to the angle $\tan\xi = 1/\sqrt{2}$, characteristic of tetrahedral bonding.

Within the electric dipole approximation, the linear absorption spectrum for excitation from the ground state $|\mu\rangle$ to an excited state $|\boldsymbol{\eta}(E)\rangle$, with a core-level electron promoted to fill a vacant discrete or continuous state, is

$$\gamma(E) = -4\pi\rho e^2 q \int_{E_\eta} \frac{(\Gamma/2)|\boldsymbol{\varepsilon}\cdot\langle\mu|\boldsymbol{r}|\boldsymbol{\eta}(E_\eta)\rangle|^2}{(E_\mu + E - E_\eta)^2 + (\Gamma/2)^2}\,\mathrm{d}E_\eta \tag{13}$$

where $\boldsymbol{\varepsilon}$ is the polarization unit vector and Γ is the core-hole width. We will consider, for the time being, only the 'white-line' feature of the absorption spectrum, which we assume to arise from excitation of a 1s core level to a vacant anti-bonding σ^*-orbital, of mixed s–p character, at the bromine site. One can therefore write

$$\gamma \propto |\boldsymbol{\varepsilon}\cdot\langle\psi_s|\hat{\boldsymbol{r}}|\psi_{\sigma^*}\rangle|^2 \tag{14}$$

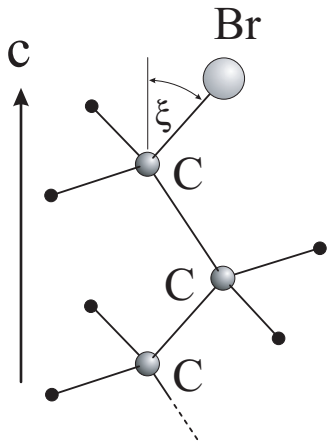

Figure 1. A bromine atom at one end of an α, ω-dibromoalkane ($Br(CH_2)_nBr$) molecule. Tetrahedral sp^3 hybridized orbitals are represented by black lines; black spheres are hydrogen atoms. The arrow indicates the direction of the crystal c-axis.

(This figure is in colour only in the electronic version)

where we consider only the angular part of the integral, which contains all the polarization dependence. It is a reasonable approximation to assume rotation symmetry around the axis defined by the vector $\hat{\boldsymbol{m}}$, which lies along the C–Br bond, and one can write the angular part of the σ^*-orbital as

$$\psi_{\sigma^*} = \alpha + \beta \hat{\boldsymbol{r}} \cdot \hat{\boldsymbol{m}} \tag{15}$$

where the first and second terms are the (isotropic) 4s amplitude and the 4p amplitude, respectively. (For the special case of sp^3 hybridization, $\beta^2 = 3\alpha^2$.) One can now write a very simple expression for the polarization dependence of the 'white-line' feature:

$$\gamma = a|\boldsymbol{\varepsilon} \cdot \langle 1|\hat{\boldsymbol{r}}|\hat{\boldsymbol{r}} \cdot \hat{\boldsymbol{m}}\rangle|^2 = a\,|\boldsymbol{\varepsilon} \cdot \hat{\boldsymbol{m}}|^2 \tag{16}$$

where a is a constant and we note that, as expected, the s-like part of the orbital does not contribute to the absorption. Interestingly, the above expression is identical to the term responsible for magnetic linear dichroism and second-order resonant magnetic diffraction [5, 6, 15], which explains our choice of notation.

In Cartesian tensor form, with $\hat{\boldsymbol{m}}$ parallel to the z-axis,

$$\gamma = \begin{pmatrix} 0 & 0 & 0 \\ 0 & 0 & 0 \\ 0 & 0 & a \end{pmatrix}. \tag{17}$$

The absorption tensor for the α, ω-dibromoalkane/urea inclusion compounds, with the crystallographic c-axis along the z-direction, is obtained by first rotating by the angle, ξ, about an axis perpendicular to z, and then accounting for the dynamic disorder with respect to the c-axis by averaging over all possible orientations around that axis, resulting in

$$\gamma = \begin{pmatrix} (a/2)\sin^2\xi & 0 & 0 \\ 0 & (a/2)\sin^2\xi & 0 \\ 0 & 0 & a\cos^2\xi \end{pmatrix}. \tag{18}$$

The ratio of attenuation coefficients, for the photon linear polarization perpendicular and parallel to the c-axis, is then

$$R_\gamma = \frac{\gamma_{22}}{\gamma_{33}} = \frac{1}{2}\tan^2\xi \tag{19}$$

which, for $\tan\xi = 1/\sqrt{2}$, gives

$$R_\gamma = \tfrac{1}{4}. \tag{20}$$

Taking the *average* absorption coefficient as γ, we can write the maximum and minimum coefficients as $\gamma_1 = \frac{8}{5}\gamma$, $\gamma_2 = \frac{2}{5}\gamma$, giving a principal transmittance ratio, which depends on the polarizer thickness, of

$$R_t = \mathrm{e}^{-(\gamma_1-\gamma_2)t} = \mathrm{e}^{-\frac{6}{5}\gamma t}. \tag{21}$$

In reality, this value is closer to unity than the above model would indicate, due largely to the fact that, even at the centre of the 'white-line' resonance, a component of the attenuation arises from isotropic processes. This is discussed in the next section.

3. Production and characterization of α,ω-dibromoalkane/urea polarizers

The 1,10-dibromodecane/urea inclusion compound (containing 1,10-dibromodecane ($Br(CH_2)_{10}Br$) as the guest species) was prepared from commercially available reagents using the following method. Separate saturated solutions of 1,10-dibromodecane in 2-methylbutan-2-ol and urea in methanol were prepared under ultrasonic agitation at 328 K. These solutions were then mixed in a conical flask, in amounts corresponding to an excess of 1,10-dibromodecane (excess with respect to the expected guest/host molar ratio in the inclusion compound). Crystals that precipitated immediately were dissolved by adding additional methanol. The flask was then transferred to an incubator and cooled systematically from 328 to 288 K over a period of 24 h and then maintained at 288 K for several days. When sufficiently large crystals had grown, they were collected and washed with 2,2,4-trimethylpentane. The crystals were long hexagonal needles, and their behaviour in the polarizing microscope was consistent with their assignment to the hexagonal crystal system. Powder x-ray diffraction data recorded at ambient temperature confirmed that these crystals had the hexagonal host structure of the conventional urea inclusion compounds, and indicated that the samples did not contain any significant amount of the 'pure' crystalline phase of urea (the crystal structure of which differs substantially from that of urea inclusion compounds).

The crystals of the 1,10-dibromodecane/urea inclusion compound grown by this technique are of high quality, but tend to be long (∼5–10 mm along the *c*-axis) and thin (∼0.3–0.5 mm). Preliminary absorption measurements indicated that the attenuation length (roughly the thickness required for an optimized polarizer) is around 0.5 mm near the bromine K edge. An ideal polarizer would therefore be a platelet of this thickness, several mm across, with the *c*-axis parallel to the large face. A crude, but very effective, technique for producing devices of the required geometry and orientation was found by aligning 10–20 crystals in a rectangular PTFE gasket, adding a drop of cyanoacrylate glue, and crushing the mixture in a press with a force of $\sim 10^4$ N. The resulting material formed apparently uniform platelets of the desired size and thickness, and linear dichroism measurements showed that the polarization, at the molecular level, was remarkably close to that found in individual crystals.

Sample characterization and dichroism spectra were measured on SRS Station 16.3, Daresbury Laboratory [16]. Figure 2 shows the attenuation through such a device, as a function of energy (close to the bromine K edge), and sample orientation with respect to the horizontal plane of photon polarization. A very strongly dichroic resonance is clearly apparent close to the edge, which exhibits a factor of two attenuation variation with polarization, with an average attenuation around a factor of three. These parameters indicate a very effective x-ray polarizer. The sample uniformity, examined by scanning a small (0.1×0.1 mm) x-ray beam over the area of the polarizer, at the absorption edge, was found to be ∼10%. Although traces of the

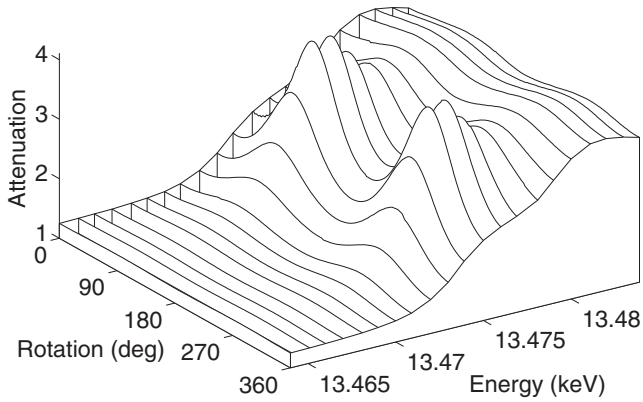

Figure 2. Attenuation ($e^{+\gamma t}$) by a 1,10-dibromodecane/urea filter near the bromine K edge, as a function of energy, and orientation with respect to the incident beam linear polarization.

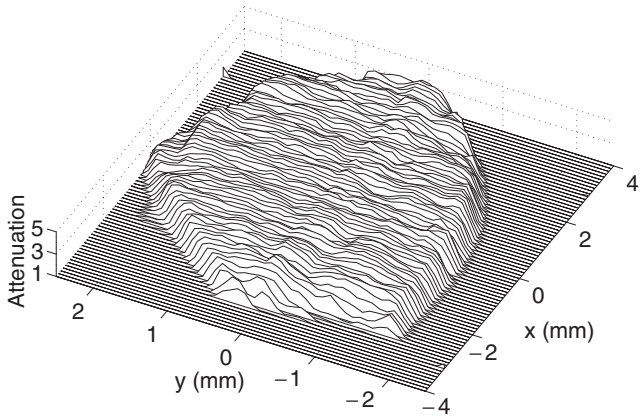

Figure 3. A map of the attenuation by the 1,10-dibromodecane/urea filter, near the bromine K edge. The remnant outline of a crystal is just visible, although the attenuation variations amount to less than 10%.

constituent crystals can just be seen (figure 3), inhomogeneities on this scale do not constitute a significant source of experimental error in polarization measurement, partly due to averaging over relatively large ($\sim$1 mm^2) beam sizes.

A key issue concerning the use of bromine-containing polarizers is stability. During the reported measurements, no deterioration was observed due to radiation damage. Moreover, there was no obvious difference between the original spectra, and measurements made after storing the prepared filters in air, at room temperature, for 15 months. The latter absorption spectra (figure 4), show very strong dichroism in the near-edge structure, and weaker dichroism in the EXAFS region. Figure 4 also shows the ratio of attenuation coefficients for perpendicular and parallel polarization, reaching a minimum value of $R_\gamma = \gamma_\perp/\gamma_\parallel \approx 0.65$, which can be compared to the value of $1/4$ in equation (20). This apparent discrepancy arises from the fact that, even at the centre of the 'white-line' feature, much of the absorption arises from processes which exhibit little or no dichroism, and thus reduce the effectiveness of the polarization filter. This is a fundamental limitation, resulting largely from the core-hole lifetime broadening, and is unlikely to be addressed by a different choice of material. However, it is interesting to

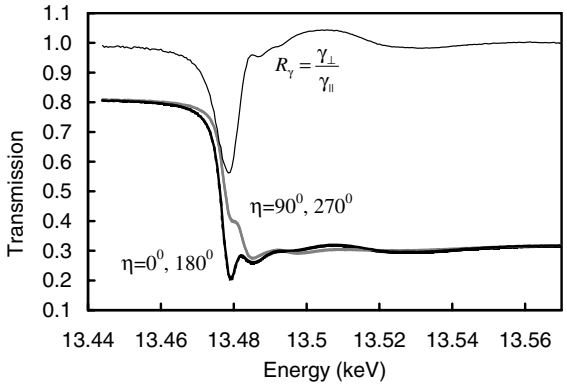

Figure 4. K-edge transmission spectra through the 1,10-dibromodecane/urea filter. Data taken with linear polarization parallel to the c-axis with ($\eta = 0^\circ$ and 180°) are shown superimposed and are discernible only as a single black line. Similarly, the perpendicular ($\eta - 90^\circ, 270^\circ$) polarization settings are seen as a single grey line. Also shown is the ratio (R_γ) of attenuation coefficients with perpendicular and parallel polarization (thin black line), which has a minimum value of ∼0.56. Measured 15 months after the original experiments, these data confirm the stability of the polarizers.

speculate on the likely improvement afforded by aligning the C–Br bond parallel to the crystal c-axis. To this end, we add an isotropic (scalar) term, b, to the absorption tensor which, after averaging over bond angles (an operation that does not affect the isotropic part), becomes

$$\gamma = \begin{pmatrix} (a/2)\sin^2\xi + b & 0 & 0 \\ 0 & (a/2)\sin^2\xi + b & 0 \\ 0 & 0 & a\cos^2\xi + b \end{pmatrix}. \tag{22}$$

Equating the attenuation coefficient ratio from this model with the measured value,

$$R_\gamma = \frac{\gamma_{22}}{\gamma_{33}} = \frac{\sin^2\xi + 2b/a}{2\cos^2\xi + 2b/a} = 0.56 \tag{23}$$

and taking $\tan\xi = \sqrt{1/2}$, one obtains $a/b \approx 2.1$, i.e., the dichroic amplitude is roughly twice that of the isotropic amplitude. For a situation in which the C–Br bond lies along the c-axis, the absorption tensor would become

$$\gamma = \begin{pmatrix} b & 0 & 0 \\ 0 & b & 0 \\ 0 & 0 & a+b \end{pmatrix} \tag{24}$$

which, with the above value for the ratio a/b, gives $R_\gamma = 0.32$. We therefore conclude that such a polarization filter, in which the C–Br bond lies along the c-axis, could be almost twice as effective as the present device. Beyond this, further significant improvement, at least with bromine-based materials, seems unlikely.

4. Magnetic diffraction from holmium

Holmium displays antiferromagnetic spiral ordering below $T_N \sim 132$ K, and possesses a large (∼10 μ_B) magnetic moment with spin/orbital ratios expected, and observed [2], to be very close to Hund-rule predictions. A holmium crystal is therefore an ideal material for testing new techniques for measuring linear polarization following non-resonant magnetic x-ray diffraction.

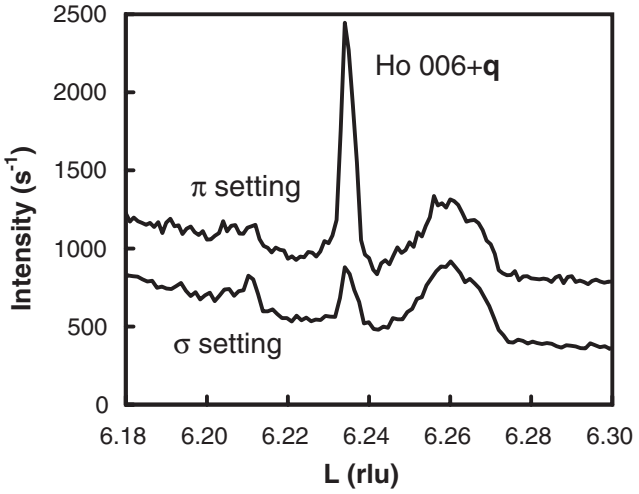

Figure 5. Diffraction patterns recorded around the Ho 0 0 6+τ magnetic peak, with the polarization filter set to transmit horizontal (σ) and vertical (π) polarization states. The data are normalized to the (non-rotated) background and offset for clarity. The intensity scale corresponds to the detector count rates for the σ-setting.

The present measurements were performed on the XMaS UK CRG beamline at the ESRF [17], with the sample cooled to $T = 50$ K by a closed-cycle cryostat, mounted on a large multi-axis diffractometer. Scattering was in the vertical plane throughout, with the incident beam polarized horizontally. Using a 1 mm vertical slit gap at the Si 111 monochromator position (∼22 m from the source), the polarization and energy width were calculated at 13.5 keV to be $P_3 \sim 0.966$ and $\Delta E \sim 4.5$ eV, respectively. The dichroic polarizer was mounted on a small rotary table, immediately in front of a germanium solid-state detector. Measurements were carried out on seven magnetic reflections, of type $0\,0\,L \pm \tau$ and $\bar{2}\,1\,L \pm \tau$, with an azimuthal angle for the latter of $\psi = 90^\circ$ (defined in section 2).

At $T = 50$ K, weak magnetic reflections were observed, corresponding to $\tau \sim 0.24$ (units of c^*), situated between two weak charge peaks (while the latter are reminiscent of magnetically induced strain peaks, their positions suggest that they originate from impurity phases). L-scans showing a pair of magnetic and charge peaks are shown in figure 5, measured with the polarizer set to transmit either σ- or π-polarized light. From these plots, one can clearly see that the broader peak on the right has the same unrotated σ-polarization as the background, whereas the narrow peak is predominantly π-polarized, and is identified as a magnetic reflection. Thus, a quick and simple measurement can provide valuable *qualitative* information about the nature of the diffraction peaks.

Quantitative investigations of the diffracted beam polarization can be performed more precisely by measuring the variation of intensity through the polarizer as it is rotated about the beam direction (figure 6). After subtracting background curves from positions either side of a magnetic peak, the data can be fitted to the cosine function in equation (10) to extract P_3'. Polarizer curves for the background signals, assumed to follow equation (12), serve as the reference data required to characterize the polarizers, and give $\Phi \sim 0.35$. It should be noted that a disadvantage of using the background signal as the main polarizer calibration is that there is a relatively large contribution from inelastic (mainly Compton) scattering, for which the polarizer is not effective. A correction of around 10% was required to account for

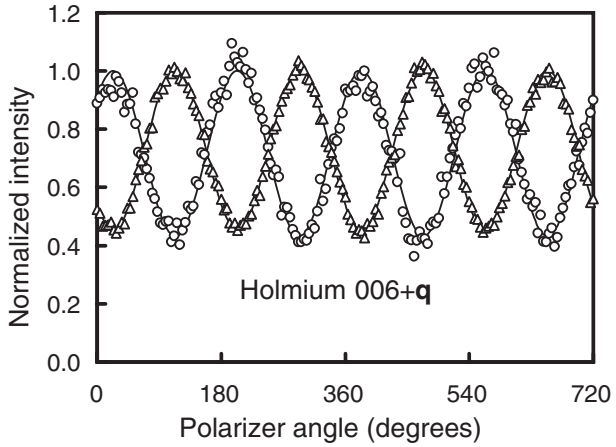

Figure 6. Intensity modulations upon rotating the polarization analyser. The circles correspond to the magnetic $(0\,0\,6+\tau)$ peak intensity, and triangles to the charge-scattering background.

this, based on the variation in the effective polarization with scattered intensity, assuming the inelastic contribution to be constant. In retrospect, it would have been better to have used the strong Bragg peaks to characterize the polarizer.

The measured linear polarization for $0\,0\,2+\tau$, $0\,0\,4+\tau$, $0\,0\,6+\tau$, $\bar{2}\,1\,2+\tau$, $\bar{2}\,1\,4+\tau$, $\bar{2}\,1\,6+\tau$, and $\bar{2}\,1\,6-\tau$ magnetic reflections is plotted in figure 7, along with the results of the calculations described in section 2, using tabulated magnetic form factors calculated from Dirac–Fock theory [18]. In order to test experimental reproducibility, a total of thirteen measurements were made, with three different polarizers. Differences between pairs of results for each reflection, indicative of the total experimental errors, are remarkably small. While experimental results are close to the calculated values, some of the residual differences appear to be statistically significant. Further measurements would be required in order to make a definitive comment on any departure from the theoretical curves.

5. Discussion and conclusions

The results reported here show clearly that linear polarization analysis can be performed very effectively with dichroic polarizers and, specifically, polarizers based on α,ω-dibromoalkane/urea inclusion compounds. There are some disadvantages compared to conventional diffraction-based techniques: chiefly, the transmittance ratios are modest, and the devices only work well within a few eV of a single absorption edge resonance energy. The latter immediately precludes dichroic polarizers from use in most resonant scattering measurements. However, for experiments in which the wavelength can be chosen to match the polarizer—non-resonant magnetic diffraction being the most obvious example—there are a number of very important advantages, which include: high average transmittance, insensitivity to beam divergence (no rocking required), simplicity of construction and use, and low cost.

The present device based on α,ω-dibromoalkane/urea inclusion compounds gives a very strong polarization dependence of around a factor of two in the attenuation coefficient at the peak of the dichroic resonance. Other materials may provide further improvements, and we have shown that an enhancement of almost a factor of two may be possible for a material in which all the bonds involving bromine are parallel. Beyond this, additional significant gains seem unlikely. The polarizer uniformity is also an issue for potential improvement. Ideally,

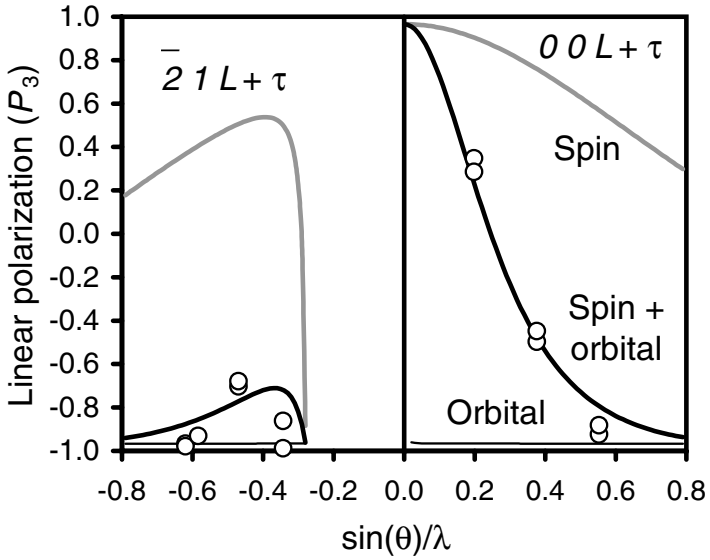

Figure 7. Measured and calculated values for the linear polarization of a series of $0\,0\,L \pm \tau$ and $\bar{2}\,1\,L \pm \tau$ magnetic reflections. The latter are displayed on a negative momentum-transfer scale for clarity. For most reflections, two independent measurements are shown, taken with different polarizers. Calculated values (thick black lines) assume Hund-rule moments. Calculations for pure spin magnetism (grey lines) and pure orbital magnetism (thin black lines) are shown for illustration.

one would cut or grow a large single crystal to the required thickness, rather than relying on the present crushing technique, and some progress in this area has already been made.

Another important issue is the choice of photon energy, and hence absorption edge. For the present case of holmium, with a large orbital/spin ratio, the sensitivity of the linear polarization to $l(k)/s(k)$ is highest for the low-order reflections, becoming less sensitive at high k. Measurements at higher energies would enhance the sensitivity for higher-order reflections. One might then find advantage in using a polarizer based, for example, on the iodine K edge close to 33 keV [7]. α, ω-diiodoalkane/urea inclusion compounds, may well prove useful for such measurements. For magnetic materials with small orbital/spin ratios, such as the 3d compounds, slightly lower photon energies are likely to be advantageous, and one might look towards polarizers based on lighter absorbing atoms.

In conclusion, we have shown that dichroic x-ray polarizers can provide high-quality linear polarization analysis, with important advantages over conventional diffraction-based techniques, especially for non-resonant magnetic diffraction. Such devices may well play an important role in future measurements to determine spin and orbital densities in antiferromagnetic crystals.

References

[1] Collins S P, Laundy D and Guo G Y 1993 *J. Phys.: Condens. Matter* **5** L637–42
[2] Gibbs D, Grübel G, Harshman D R, Isaacs E D, McWhan D B, Mills D and Vettier C 1991 *Phys. Rev.* B **43** 5663–81
[3] Langridge S *et al* 1997 *Phys. Rev.* B **55** 6392–8
[4] Fernandez V, Vettier C, de Bergevin F, Giles C and Neubeck W 1998 *Phys. Rev.* B **57** 7870–6
[5] Lovesey S W and Collins S P 1996 *X-Ray Scattering and Absorption by Magnetic Materials* (Oxford: Clarendon)
[6] Hill J P and McMorrow D F 1996 *Acta Crystallogr.* A **52** 236–44
[7] Collins S P 1997 *Nucl. Instrum. Methods* B **129** 289–96

[8] Krone W, Wortmann G, Frank K H, Kaindl G, Menke K and Roth S 1984 *Solid State Commun.* **52** 253–6
[9] Heald S M and Stern E A 1978 *Phys. Rev.* B **17** 4069–81
[10] Harris K D M and Thomas J M 1990 *J. Chem. Soc. Faraday Trans.* **86** 2985–96
[11] Harris K D M, Smart S P and Hollingsworth M D 1991 *J. Chem. Soc. Faraday Trans.* **87** 3423–9
[12] Yeo L and Harris K D M 1997 *Acta Crystallogr.* B **53** 822–30
[13] Guillaume F, Smart S P, Harris K D M and Dianoux A-J 1994 *J. Phys.: Condens. Matter* **6** 2169–84
[14] Aliev A E, Smart S P, Shannon I J and Harris K D M 1996 *J. Chem. Soc. Faraday Trans.* **92** 2179–84
[15] Hannon J P, Trammell G T, Blume M and Gibbs D 1988 *Phys. Rev. Lett.* **61** 1245–8
[16] Collins S P, Murphy B M, Tang C C, Miller M C and Oszlanyi G 1999 *J. Phys. D: Appl. Phys.* **32** A81–3
[17] Brown S D *et al* 2001 *J. Synchrotron Radiat.* **8** 1172–81
[18] Brown P J 1999 *International Tables for Crystallography* (Dordrecht: Kluwer) pp 450–7